Measurement report: Impact of cloud processes on secondary organic aerosols at a forested mountain site in southeastern China

Zijun Zhang[1,2], Weiqi Xu[1,*], Yi Zhang[1,2], Wei Zhou[1], Xiangyu Xu[1,2], Aodong Du[1,2], Yinzhou Zhang[1], Hongqin Qiao[3], Ye Kuang[3], Xiaole Pan[1], Zifa Wang[1,2], Xueling Cheng[1], Lanzhong Liu[4], Qingyan Fu[5], Douglas R. Worsnop[6], Jie Li[1], Yele Sun[1,2,*]

[1]State Key Laboratory of Atmospheric Boundary Layer Physics and Atmospheric Chemistry, Institute of Atmospheric Physics, Chinese Academy of Sciences, Beijing 100029, China
[2]College of Earth and Planetary Sciences, University of Chinese Academy of Sciences, Beijing 100049, China
[3]Institute for Environmental and Climate Research, Jinan University, Guangzhou 511143, China
[4]Shanghuang Eco-Environmental Observatory of Chinese Academy of Sciences, Jinhua 321203, China
[5]Shanghai Environmental Monitoring Center, Shanghai 200235, China
[6]Aerodyne Research Inc., Billerica, Massachusetts 01821, United States

Correspondence to: Weiqi Xu (xuweiqi@mail.iap.ac.cn), Yele Sun (sunyele@mail.iap.ac.cn)

Abstract. Aerosol particles play critical roles in climate and human health. However, aerosol composition and evolution, particularly secondary organic aerosols (SOA), and its interaction with clouds in high-altitude background areas in China remain less understood. Here we conducted real-time measurements of submicron aerosols (PM_1) using aerosol mass spectrometers at a forested mountain site (1128 m a.s.l.) in southeastern China in November 2022. The average (± 1σ) PM_1 mass concentration was 4.45 ± 6.51 μg m^{-3}, which was ubiquitously lower than those at other mountain sites in China. Organic aerosol (OA) constituted the largest fraction of PM_1 (42.9 %) and was dominantly secondary as indicated by the high oxygen-to-carbon (O/C) ratio (0.85–0.96) and carbon oxidation state (0.21–0.49). Back trajectory analysis revealed that higher concentrations of PM_1 were mainly associated with the transport from the western and southwestern regions. Notably, the remarkably enhanced PM_1 concentrations observed during daytime on cloudless days were identified to be likely produced from cloud evaporation. Positive matrix factorization resolved two distinct OOA factors, i.e., less oxidized oxygenated OA (LO-OOA) and more oxidized OOA (MO-OOA). While MO-OOA was scavenged efficiently during cloud events, cloud evaporation was found to release a significant amount of LO-OOA from airmass transported from polluted regions. The distinct increase of OA/ΔCO (CO after subtracting the background level) with the decrease of O/C during the cloud evaporative period further demonstrates that OA remained in cloud droplets are generally in a moderate oxidation state. Moreover, organic nitrates were also estimated and showed a higher contribution to the total nitrate during the cloudy period (27 %) than the evaporative period (3 %). Overall, our results demonstrate the importance of SOA and the influences of cloud processes in regional mountain areas in southeastern China.

1 Introduction

Aerosol particles play essential roles in regional and global climate (Ramanathan et al., 2001; Kanakidou et al., 2005), as well as air pollution (Huang et al., 2014) and public health (Kampa and Castanas, 2008). Submicron aerosol (PM_1) from both natural and anthropogenic sources can be transported to the upper level of atmospheric boundary layer or even lower free troposphere through convection and frontal uplift (Monks et al., 2009; Huang et al., 2020; Carbone et al., 2014). At high altitudes, aerosol species can be transported over longer distances, depending on their particle sizes and compositions (Pokorná et al., 2022; Tang et al., 2016; Zhong et al., 2022), and the aging processes during transport results in continuous changes in chemical and physical properties (Calvo et al., 2013; Hallquist et al., 2009). Aerosols can have an important impact on CCN properties at high altitudes where atmospheric conditions favour the formation of clouds, thereby affecting the lifetime and optical properties of clouds through aerosol-cloud interactions (Haywood and Boucher, 2000; Asmi et al., 2012; Rejano et al., 2021). On the other hand, aerosol-cloud interactions also modify the chemical composition of aerosols within cloud droplets. This modification, in turn, affects the characteristics of surrounding aerosols after the cloud has evaporated (Roth et al., 2016). As a result, measurements of high-altitude regional aerosols are of great importance for a better understanding of aerosol-cloud interactions and their impacts on air pollution and climate.

Mountain sites are crucial platforms for studying aerosol characteristics over regional scales and the influences of diverse emission sources (e.g., biomass burning, industrial process, and biogenic emissions) and atmospheric processes (e.g., in-cloud processing, new particle formation). Compared to balloon and aircraft observations, mountain sites have advantages in continuous and long-term observations because of low cost, stable geographic location, and accessibility for instrument maintenance. In addition, the different meteorological conditions at mountain sites can have great impacts on aerosol formation, aging, and scavenging patterns. For example, Gao et al. (2023) showed that cloud processes can promote the formation of secondary organic aerosol (SOA) by multiphase oxidation. Li et al. (2013) found that high relative humidity (RH) at Mt. Hua can lead to a reduction in particle acidity, and thus reduce the formation of biogenic SOA by suppressing the acid-catalysis reaction. Chen et al. (2021) reported that fog scavenging was more efficient towards particles with aerodynamic diameter larger than 700 nm in Taiwan mountain regions, while smaller particles remained growth through the process of gas-to-aqueous partitioning. Although several mountain stations have been established in China to gain more information on the chemical composition and sources (Zhang et al., 2018; Zhang et al., 2019; Du et al., 2015; Zhang et al., 2014), optical properties (Wang et al., 2015), and hygroscopic properties of aerosols (Ding et al., 2021), most of these studies are mainly conducted on Qinghai-Tibetan Plateau and in Northern China Plain (NCP), while the studies in southeastern China remain limited.

In this work, a high-resolution time-of-flight aerosol mass spectrometer (AMS hereafter) and a quadruple aerosol chemical speciation monitor (ACSM hereafter) were deployed at a forested mountain site in southeastern China. The chemical composition and properties of PM_1 are characterized, the elemental composition and oxidation state of OA are determined, and the potential transport pathways of PM_1 are also investigated using back trajectory analysis. Furthermore, the effect of

cloud processes on aerosol species is discussed. The sources of organic aerosol are investigated using positive matrix factorization (PMF) analysis of combined high-resolution organic and inorganic aerosol mass spectra. Particularly, particulate organic nitrates (ONs) are determined and quantified based on PMF results.

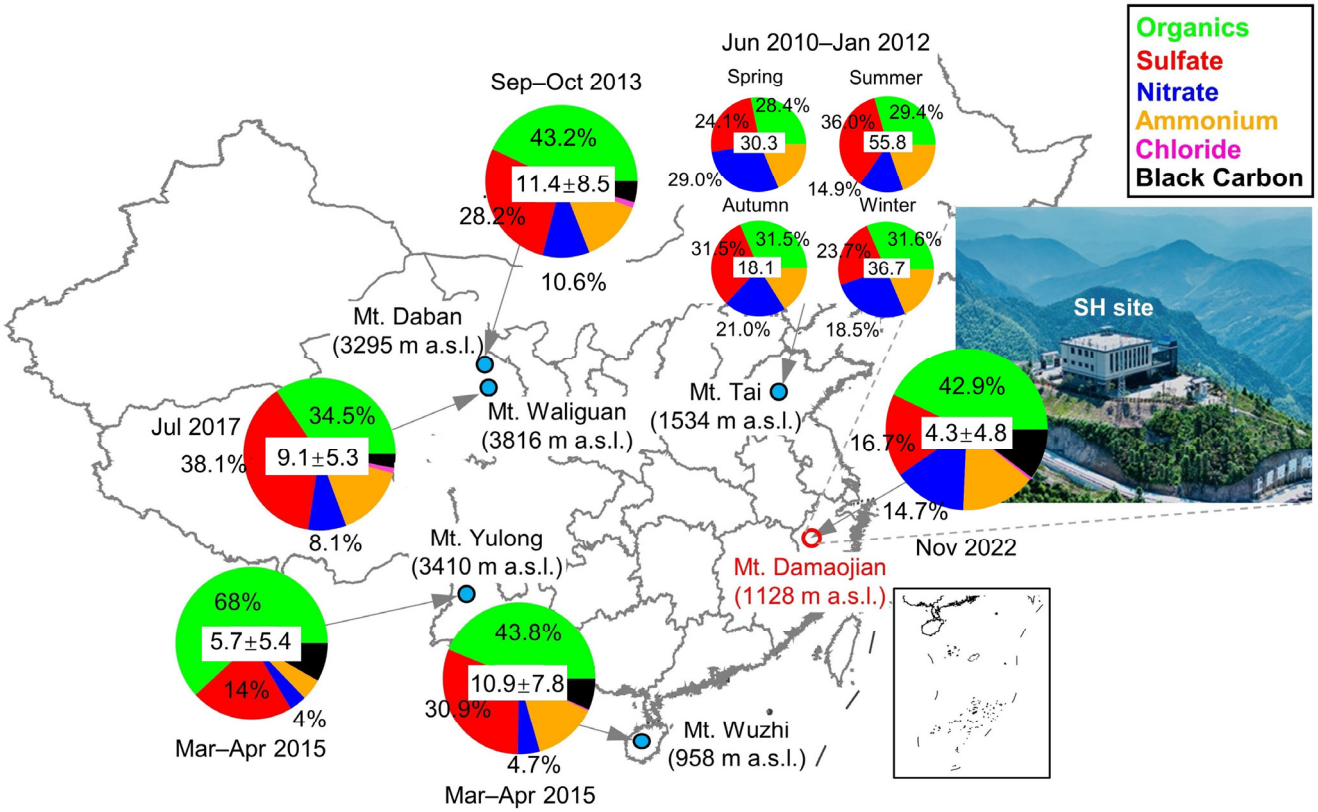

Figure 1. Location of the sampling site (Mt. Damaojian, red circle on the map). The mean concentration (μg m^{-3}) and chemical composition of submicron aerosols (NR-PM_1+ BC) measured at selected mountain sites in China are also shown. Note that BC and chloride are not accounted for Mt. Tai due to the lack of measurement or data in the relevant study. Detailed information of these sampling sites is presented in Table S1 in the Supplement.

2 Methods

2.1 Site and instrumentation

The campaign was carried out from 1 November to 30 November 2022 at Shanghuang Eco-Environmental Observatory of Chinese Academy of Sciences (SH), located at Mt. Damaojian (119.51°E, 28.58°N, 1128 m a.s.l.) in Wuyi County, Zhejiang Province (Fig. 1). This site is a typical background site in southeastern China that is surrounded by mountains and forests, and there are no strong local anthropogenic sources nearby.

PM_1 species were measured using a suite of real-time instruments with 1−20 min time resolution, including an AMS operated under the V-mode and a quadrupole ACSM for non-refractory (NR)-PM_1 composition, together with a seven-wavelength Aethalometer (AE33, Magee Scientific Corp.) for equivalent black carbon (BC) mass concentration. The AMS measurements were only conducted during two periods (15−20 November and 24−28 November, respectively) in this study due to the malfunction of the instrument. Briefly, aerosol particles were sampled into an air-conditioned room through stainless steel tube (O.D.: 1/4 inch), and the residence time was estimated as 5 s. A nafion dryer was placed upstream of the ACSM and AMS to remove the moisture, after that, aerosol particles were sampled into AMS, ACSM, and AE33, respectively. Because there was no size cutoff in front of the sampling line, the AMS and ACSM may report slightly higher concentrations than expected because of measuring some cloud droplets larger than 2.5 μm. According to a previous study during three fog episodes at a rural site in North China Plain, the influence of fog droplets on submicron aerosol measurements was less than 20% (Kuang et al., 2024). Simultaneously, air pollutants including NO_x, O_3 were measured by a suite of gas analyzers (Thermo Scientific Inc., USA), $PM_{2.5}$ and PM_{10} were measured using continuous ambient particulate monitors with $PM_{2.5}$ and PM_{10} cutoff before the sampling inlet (Model 5014i, Thermo Scientific., USA), and CO was measured by a Picarro greenhouse gas analyzer (G2401, Picarro Inc., USA). Meteorological parameters containing temperature (*T*), RH, wind speed (WS), wind direction (WD), and pressure (*P*) were measured by an automatic weather station. In addition, (PDR). More details and descriptions of the instruments and data are provided in Table S1.

2.2 Data analysis

2.2.1 ACSM and AMS

ACSM data were analyzed using ACSM standard data analysis software (v2.5.13) and AMS data were analyzed using SQUIRREL v1.65F and PIKA v1.25F. A composition-dependent collection efficiency (CDCE) was applied to the ACSM/AMS data according to Middlebrook et al. (2012). Elemental analysis of high-resolution mass spectra (HRMS) was performed using the "Improved-Ambient" (I-A) method (Canagaratna et al., 2015). The default relative ionization efficiency (RIE) values of 1.1, 1.4, and 1.3 were applied for nitrate, organics, and chloride (Canagaratna et al., 2007; Nault et al., 2023). According to the ion efficiency (IE) calibration results using ammonium sulfate, the RIE values of ammonium and sulfate were 5.05 and 0.73 for ACSM, and 5.26 and 1.28 for AMS, respectively. Detailed comparison of the concentrations of NR-PM_1 species measured by AMS and ACSM are shown in Fig. S1. The ACSM data during the sampling period was corrected by using the regression coefficients between ACSM and AMS. As shown in Figs. S1g and h, after this adjustment, the concentrations of NR-PM_1 tracked well with $PM_{2.5}$ (r^2 = 0.60 and slope = 0.48 for ACSM, r^2 = 0.93 and slope = 0.54 for AMS respectively) and PM_{10} ((r^2 = 0.53 and slope = 0.27 for ACSM, r^2 = 0.99 and slope = 0.39 for AMS respectively) measured by the particle monitor, suggesting that the AMS/ACSM quantification was reasonable.

PMF Evaluation Tool (PET v3.04) was employed to further deconvolve the HRMS derived from AMS into different source factors following the procedures reported by Ulbrich et al. (2009) and Zhang et al. (2011). In addition to organic fragment

ions, the major fragment ions of inorganic species, i.e., SO^+ (*m/z* 48), SO_2^+ (*m/z* 64), SO_3^+ (*m/z* 80), HSO_3^+ (*m/z* 81), $H_2SO_4^+$ (*m/z* 98) for sulfate, NO^+ (*m/z* 30), NO_2^+ (*m/z* 46) for nitrate, NH^+ (*m/z* 15), NH_2^+ (*m/z* 16), NH_3^+ (*m/z* 17) for ammonium, and Cl^+ (*m/z* 35), HCl^+ (*m/z* 36) for chloride were also included into the HR data and error matrices for PMF. A more detailed description of the procedures was given in Sun et al. (2012). After checking the key diagnostic plots (Fig. S2), mass spectra, and the correlations with related tracers, a four-factor solution was considered as the optimal solution in this study (Text S1).

2.2.2 Estimation of organic nitrates

ONs were estimated from the PMF results (Zhang et al., 2011; Xu et al., 2015). Briefly, NO_x^+ (i.e., NO^+ and NO_2^+) are major fragments of nitrate functionality ($-ONO_2$), which can be referred to as the total nitrate measured by AMS. Combining inorganic with organic mass spectra in PMF, NO^+ and NO_2^+ can be separated into different organic aerosol (OA) factors and an inorganic nitrate aerosol factor (NIA). According to previous studies, the ratios of NO^+/NO_2^+ for ONs are approximately 2.25–3.7 times higher than pure NH_4NO_3 (Fry et al., 2013; Fry et al., 2009). Consistently, the PMF results in our study (Fig. 7) show that the average NO^+/NO_2^+ ratios of LO-OOA and MO-OOA were 13.19 and 11.2, falling within the range of ONs. In contrast, a NO^+/NO_2^+ ratio of 3.56 was observed for NIA, reflecting its characteristics of inorganic nitrates. Therefore, the PMF analysis of nitrate is reasonable, and based on this result, the mass concentration of ONs ($NO_{3,org}$) can be calculated by summing these two ion signals distributed in all OA factors as follows:

$$NO_{3,org} = NO^+_{org} + NO^+_{2,org} \quad (1)$$

$$NO^+_{org} = \sum([\text{OA factor}]_i \times f_{NO^+,i}) \quad (2)$$

$$NO^+_{2,org} = \sum([\text{OA factor}]_i \times f_{NO_2^+,i}) \quad (3)$$

where $[\text{OA factor}]_i$ represents the mass concentration of OA factor *i* resolved by PMF, $f_{NO^+,i}$ and $f_{NO_2^+,i}$ are the mass fractions of NO^+ and NO_2^+ in OA factor *i*, respectively.

2.2.3. Backward trajectory analysis

The Hybrid Single-Particle Lagrangian Integrated Trajectories (HYSPLIT) model and meteorological data from the NOAA Global Data Assimilation System (GDAS) were used to calculate 72 h backward trajectories at the SH site. The trajectory arrival time was set from 0:00 to 23:00 at 1 h intervals, and the arrival height at the site was set as 1100 m. To further show the aerosol particle concentration levels in different regions, the map contained the back trajectory (Fig. S5) was coloured by the time-averaged organic carbon surface mass concentration from the M2T1NXAER v5.12.4 dataset (0.5 × 0.625°, hourly). This dataset, part of the Modern-Era Retrospective analysis for Research and Applications version 2 (MERRA-2) model (Gelaro et al., 2017), was sourced from the NASA Giovanni website (https://giovanni.gsfc.nasa.gov).

3. Results and discussion

3.1. Mass concentration and chemical composition of submicron aerosols

Figure 2 shows the time series of meteorological parameters (*T*, RH, WD, and WS), air pollutants ($PM_{2.5}$ and CO) along with PM_1 (NR-PM_1 + BC) species during the campaign. The total PM_1 concentration varied dynamically from 0.3 μg m^{-3} to 39.8 μg m^{-3} during the whole sampling period, with an average (± 1σ) of 4.3 ± 4.8 μg m^{-3}. As shown in Fig. 1, organics accounted for the largest contribution (42.9 %) to the total PM_1 during the sampling period, followed by sulfate (16.7 %), ammonium (15.0 %), nitrate (14.7 %), BC (10.2 %), and chloride (0.5 %). In addition, BC was observed to correlate well with PM_1 and $PM_{2.5}$ (r^2 = 0.59 and 0.62, respectively), suggesting that the aerosol particles at this site may be largely influenced by the regional biomass burning plumes in the Yangtze River Delta (Zhang et al., 2015). The concentration and composition of PM_1 are quite different from those observed at other Chinese mountain sites in different seasons (Fig. 1). For example, the average PM_1 concentration here is much lower compared to Mt. Wuzhi (10.9 ± 7.8 μg m^{-3}) at a similar altitude, and is also lower than at higher altitude mountains such as Mt. Yulong (5.7 ± 5.4 μg m^{-3}) and Mt. Waliguan (9.1 ± 5.3 μg m^{-3}). Although PM_1 concentration has a strong seasonal dependence, such as in Mt. Tai, with low concentration in autumn (18.1 μg m^{-3}) and high in summer (33.5 μg m^{-3}), the average PM_1 concentration at our site is still much lower than Mt. Daban (11.4 μg m^{-3}) and Mt. Tai in the same season (autumn). Considering the occurrence of frequent cloud events during the sampling period, the low PM_1 concentration might be mainly associated with cloud scavenging, which will be further validated in subsequent sections. Notably, a relatively lower contribution of sulfate to PM_1 was observed (16.7 %) in this site compared to other mountain sites (14.0 %−38.1 %), which was likely attributed to the significant reduction of SO_2 emission in China during the past decade (Wen et al., 2023). The decrease in sulfate contribution was associated with an elevation of nitrate contribution. This shift suggests that most NH_4 will probably be in the form of ammonium nitrate which is more volatile than ammonium sulfate and thus unlikely to transport over a large scale. Notably, at Mt. Tai, even though the contributions of sulfate were high, nitrate still accounted for considerable fractions (14.9 %−29.0 %) that were comparable to this site (20.9 %). Taken together, PM_1 at this site is more likely influenced by anthropogenic emissions over a smaller regional scale, consistent with the high urban density in eastern China.

Figure 3a shows the relative contribution of each PM_1 component as a function of PM_1 concentration together with the probability density of PM_1 mass loading. The highest two frequencies of PM_1 concentrations were distributed within 0–3 μg m^{-3} and 5–8 μg m^{-3} (29.0 % and 29.8 %, respectively). The fraction of nitrate increased significantly with PM_1 concentration, and meanwhile, the fraction of organics and BC exhibited a decreasing trend. We noted that a nitrate-dominant peak of PM_1 mass loading was observed at the nighttime of 4 November (EP1, Fig. 2d), and the concentrations of organic and nitrate as a function of PM_1 mass during this event and the rest of the campaign are shown in Fig. S3. Almost all the data points with PM_1 concentrations above 20 μg m^{-3} were from this event. During EP1, a steeper slope for nitrate relative to PM_1 was found than that for organics, which was contrary to slopes during the rest period (Fig. S3). These distinct differences in slopes for nitrate and organics implied different mechanisms of PM_1 elevation during these two periods. Consequently, we also

excluded EP1 from the statistic of Fig. 3a, and the result is presented in Fig. 3b. After removing EP1, organics became the dominant contributor (> 40 %) across all PM_1 concentrations. Despite this, there was still an increasing trend for nitrate and a decreasing trend for sulfate along with increased PM_1, yet the contribution of ammonium remained relatively constant. This further supported our previous hypothesis that there was a conversion of ammonium sulfate to ammonium nitrate with the increase in PM_1 concentration. Overall, these results suggested that high levels of PM_1 at the SH site might be mainly attributed to the formation or transport of organics, meanwhile, nitrate also plays a nonnegligible role.

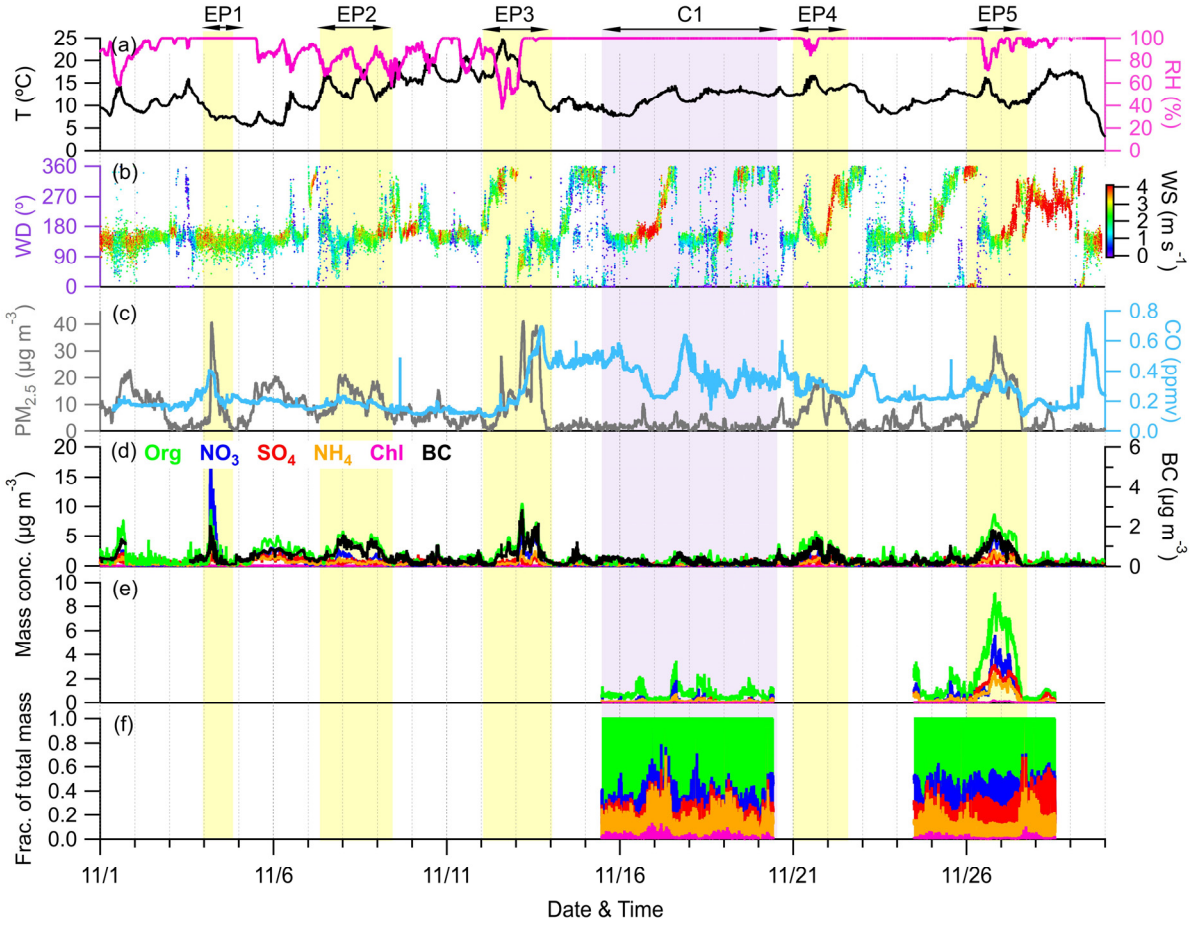

Figure 2. Time series of (a) *T* and RH; (b) WD coloured by WS; (c) mass concentration of $PM_{2.5}$ and mixing ratio of CO; (d) mass concentrations of NR-PM_1 species measured by ACSM together with BC measured by AE33; and (e, f) mass concentrations and contributions of NR-PM_1 species measured by AMS. The yellow and purple shaded areas represent six selected episodes (EP1–EP5 and C1, respectively).

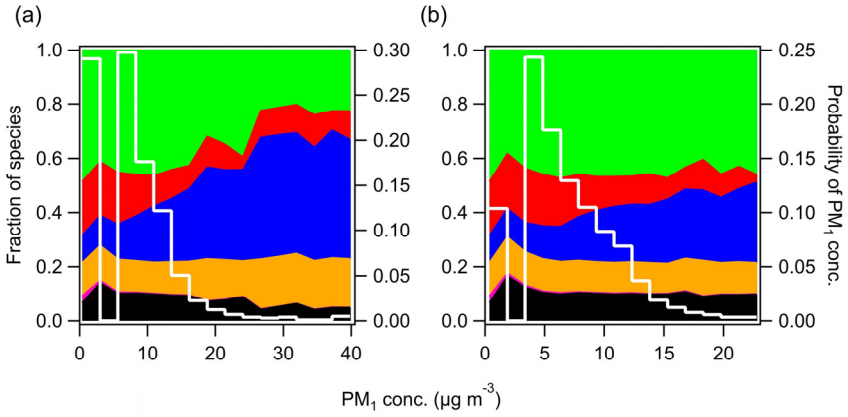

Figure 3. Variations of aerosol composition as a function of PM_1 mass concentration and the probability density of PM_1 during (a) the entire study period and (b) the period excluding EP1.

The diurnal cycles of PM_1 species, air pollutants, and meteorological parameters during the entire campaign are illustrated in Fig. S3. The mean and median values of organics and nitrate both showed distinct noon peaks at around 14:00, which could be attributed to the daytime photochemical production and the low wind speed (Tang et al., 2022; Xu et al., 2018b). In addition, these noon peaks may also be related to the development of atmospheric boundary layer, which facilitates the mixing of air masses transported from polluted areas. The high nighttime peak of nitrate was mainly due to the influences of the nitrate event on 4 November. Comparatively, sulfate, chloride, and BC showed relatively flat diurnal variations, suggesting the regional characteristics of these species (Zhang et al., 2015).

3.2 Meteorological conditions and air mass origin

The entire study period was characterized by five PM_1 episodes (EP1–EP5), as marked in Fig. 2. Meanwhile, a clean period (C1) with low PM_1 levels was also selected for comparison. The relationship between the PM_1 species concentration, meteorology, and air mass transport during these six periods is shown in Fig. 4 and Fig. S5. EP1 exhibited a nitrate-dominant PM_1 peak, with nitrate concentration rapidly increased by ~18 μg m^{-3} within an hour. In addition, a CO peak was also observed at that time, suggesting potential contributions of pollution transport to nitrate. Given the lack of anthropogenic activities near the sampling site, the enhanced nitrate concentrations likely originated from NO_x transported from adjacent towns in the northeast, as indicated by the nitrate wind polar plot (Fig. S6) showing high levels of nitrate mainly associated with northeastern wind directions. This was further supported by the back trajectory analysis, in which air masses on 4 Nov were also from the northeast. Moreover, the RH was stable at 100% during EP1, which could facilitate the heterogenous uptake of N_2O_5 and subsequent nitrate formation in the aqueous phase at night (Brown et al., 2006; Li et al., 2020).

In contrast to EP1, PM_1 in other episodes (EP2–5) were all dominated by organics. EP2 was associated with low concentrations of CO, indicating relatively slight pollution transport influence. In addition, clear and similar diurnal variation patterns were found in aerosol species and RH, suggesting that PM_1 in this period was mainly affected by the evolution of

the atmospheric boundary layer. EP3 was initiated by an organic-only increase under high temperature (~15–25 °C) and low RH (~40 %–80 %), while other aerosol species remained at very low levels. Considering the low CO levels in this period, the increasing trend of OA could be attributed to the local biogenic emissions. The concentrations of organic, together with other PM_1 species and CO, were further elevated after airmass sources shifted from southwest to northwest on 13 Nov, which may bring a large amount of aerosols from megacities such as Zhengzhou and Hangzhou to the SH site (Fig. S5c). EP4 and EP5 were two similar episodes, where PM_1 concentrations were generally associated with the changes in RH and WD. During these two periods, air masses both originated from the west and southwest, but the trajectory distances during EP5 were shorter, suggesting that the air masses transported more slowly in EP5.

Overall, although these episodes had different mechanisms of PM_1 variation, they were mostly influenced by the transport of western and southwestern air masses, indicating a substantial impact of anthropogenic emissions from big cities like Nanchang and Fuzhou. These areas are marked by higher pollution according to the organic carbon distribution in Fig. S5. However, we have also identified similar transport pathways and even higher CO concentrations during C1 (0.37 ppm on average) than EP2–5 (0.18–0.31 ppm on average), while the PM_1 concentration stayed at very low levels for the whole period. It is worth noting that PM_1 peaks in EP2−EP5 all occurred along with RH below 100 %. When the RH returned to 100 %, PM_1 concentrations gradually diminished to levels comparable to those observed during the clean period (C1). Furthermore, as shown in Fig. S7, there were notable reductions in the mean and median mass concentrations of all PM_1 species over the entire campaign, ranging between -2.6 %−44.4 % and 2.8 %−50.1 % when RH reached 100 % from conditions of lower RH, respectively. Considering the frequently occurring cloud events at this site, it was most likely that these variations of RH were affected by the cloud process, which may further play an important role in PM_1 concentrations.

Figure S8 shows the particle depolarization ratio measured by the particle lidar during EP5 and C1. During EP5, clouds were identified at ~1 km above the sampling site from 2:00 to 12:00 on 26 Nov (Fig. S8a). As expected, these clouds gradually disappeared afterward, possibly owing to strong solar radiation at noon on the mountaintop causing cloud droplet evaporation. Meanwhile, a large amount of aerosol particles (PDR = ~0.15) was released from the clouds, which exhibited a strong agreement with the timing of the PM_1 peak. These particles were then scavenged by the increased RH and strong wind (WS > 4 m s^{-1}). This cloud evaporation phenomenon was also found in urban Guangzhou, which caused remarkably enhanced nitrate mass concentration at noon (Tao et al., 2018). In contrast, no such evaporation process was observed during C1 (Fig. S8b). Instead, high PDR values were found generally at around 0 km, which means that clouds constantly existed near the sampling area during this period, coinciding with the constant 100% RH. Therefore, PM_1 transported to this site was likely to be scavenged by the cloud during C1. These findings were also evidenced by the photos taken at this site at local time ~15:00 on 19 Nov and 26 Nov, where severe cloud cover was observed in C1 (Fig. S9a), yet the weather was generally sunny and cloudless in EP5 (Fig. S9b). As a result, besides regional transport, cloud processes can also have significant impacts on aerosol particles at this site.

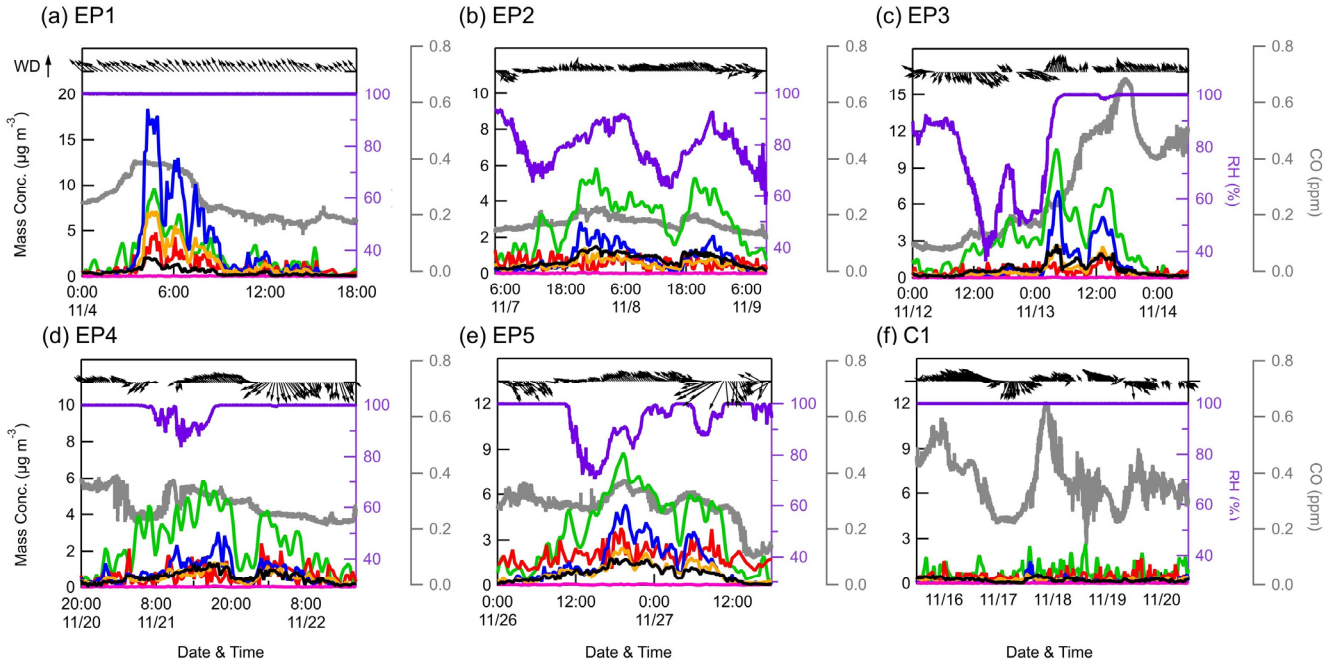

Figure 4. Temporal variations of NR-PM_1 species measured by ACSM, as well as CO, RH, WD, and WS during six case events.

3.3 Impacts of cloud processes on submicron aerosols

To further explore the impacts of cloud scavenging and cloud evaporation on aerosol characteristics, we select C1 and EP5, in which NR-PM_1 were also measured by AMS, for further investigation in this section.

3.3.1 Size distributions and composition

The average chemically resolved size distributions of NR-PM_1 during C1 and EP5 are shown in Fig. 5. Generally, all species were distributed in accumulation mode in both periods. However, a smaller peak size (300–500 nm) and broader size distribution were observed during C1 when compared to those of EP5 (~700 nm), probably owing to the wet removal of larger and hygroscopic particles in C1 (Ge et al., 2012). Also, the complex and broad size distribution observed in C1 suggests that these smaller particles are likely externally mixed with organics, which may further imply the potential formation of SOA from local biogenic sources. In contrast, the uniform size distribution across all particulate species in EP5 indicates their well-mixed and highly aged characteristics. Moreover, ammonium showed similar size distribution with sulfate and nitrate during EP5, while in C1, it was mixed mainly with sulfate and exhibited a quite different size distribution with nitrate, indicating the potential contribution of organic nitrate.

Clear differences were also found in aerosol composition during C1 and EP5. Organics were the dominant contributor to total NR-PM_1 mass during C1 (68 %), followed by nitrate (12 %), ammonium (11 %), and sulfate (8 %). In contrast, despite

the decreased contribution of organics (51 %), the mass fractions of sulfate and nitrate increased considerably during EP5 (by 9.4% and 7.0%, respectively). These changes in the mass fraction of species were attributed to the lower mass scavenging efficiency of organics than inorganic species (Gilardoni et al., 2014). The average HRMS of OA during C1 and EP5 are presented in Fig. S10. The HRMS of OA were quite similar for the two periods, with a significant peak *m/z* 44 (mainly CO_2^+). The OA was highly oxidized, with $C_xH_yO_1^+$ dominating the total OA in C1 and EP5 by 41 % and 40 %, followed by $C_xH_y^+$ (31 % and 32 %), and $C_xH_yO_2^+$ (20 % and 19 %). The contributions of the two major oxygen-containing ion fragments ($C_xH_yO_1^+$ and $C_xH_yO_2^+$) at the SH site were much higher than those at various urban or suburban sites in China, such as 37.4 % in urban Nanjing (Wang et al., 2016), and 52.9 % in suburban Lanzhou (Tang et al., 2022). Note that higher fraction of CO_2^+ (3 % higher) was found in C1 than EP5 (Fig. S10c), indicating a higher oxidation degree of OA in C1 (Xu et al., 2014). This is consistent with the higher O/C and OSc in C1 (0.96 and 0.49) than EP5 (0.85 and 0.21).

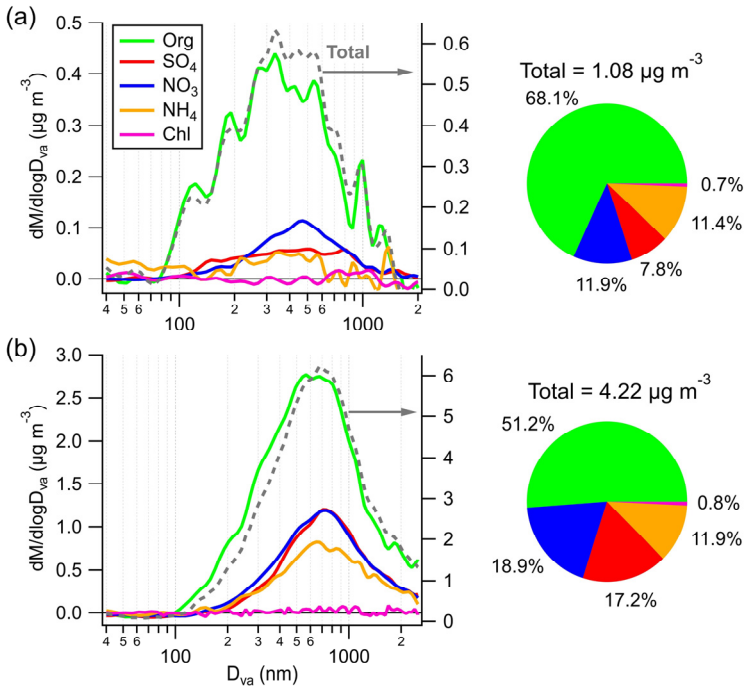

Figure 5. Averaged size distributions and chemical composition of NR-PM_1 during (a) C1 and (b) EP5.

3.3.2 Elemental ratios

Figure 6 shows the time series and box plots of N/C, H/C, OM/OC, O/C, and carbon oxidation state (OSc) of OA, as well as two ion ratios at the SH site. The hourly averaged ratios were only reported for periods with OA concentrations above 0.7 μg m^{-3}. The average N/C ratios were 0.018 for C1 and 0.027 for EP5, consistent with the higher fraction of $C_xH_yN_p^+$ in OA during EP5. OA had a slightly lower H/C ratio (1.44 vs. 1.48) and higher average ratios of O/C (0.96 vs. 0.85), OM/OC (2.42 vs. 2.29), and OSc (0.49 vs. 0.21) during C1 than those during EP5, indicating more oxidized OA during C1. The O/C

ratios were overall within the range of 0.94 ± 0.18 at regional background sites (Zhou et al., 2020), yet much higher than those observed at urban and suburban sites. These results suggest that OA at the SH site was relatively aged.

The ratio of fragment ions NO^+ (*m/z* 30) to NO_2^+ (*m/z* 46) is a good indicator for identifying the presence of ONs (Farmer et al., 2010; Lin et al., 2021). The mean ratio of NO^+/NO_2^+ in C1 was 4.9, which exceeds the value of 3.88 for pure ammonium nitrate (NH_4NO_3) obtained from the AMS IE calibration, indicating a potential contribution of ONs. Conversely, the mean NO^+/NO_2^+ in EP5 (3.9) was almost identical to that of NH_4NO_3, implying the dominance of inorganic nitrates (INs). Additionally, the $CH_2SO_2^+$ (*m/z* 79) and $CH_3SO_2^+$(*m/z* 80) ions were used as signature fragments of methanesulfonate, a typical organic sulfur species generated in marine and remote coastal regions (Chen et al., 2019). However, the mean ratios of $CH_3SO_2^+$ and $CH_2SO_2^+$ during C1 and EP5 (0.98 and 1.99, respectively) were lower than the value of 2.9 reported in previous studies for MSA, indicating the minimal contribution of MSA (Song et al., 2019). The low contributions of MSA further suggest that aerosols over this region are likely to have negligible oceanic influences. This is also consistent with the back trajectory results in section 3.2, which demonstrate that PM_1 levels at this site are dominantly influenced by continental sources in the west and southwest.

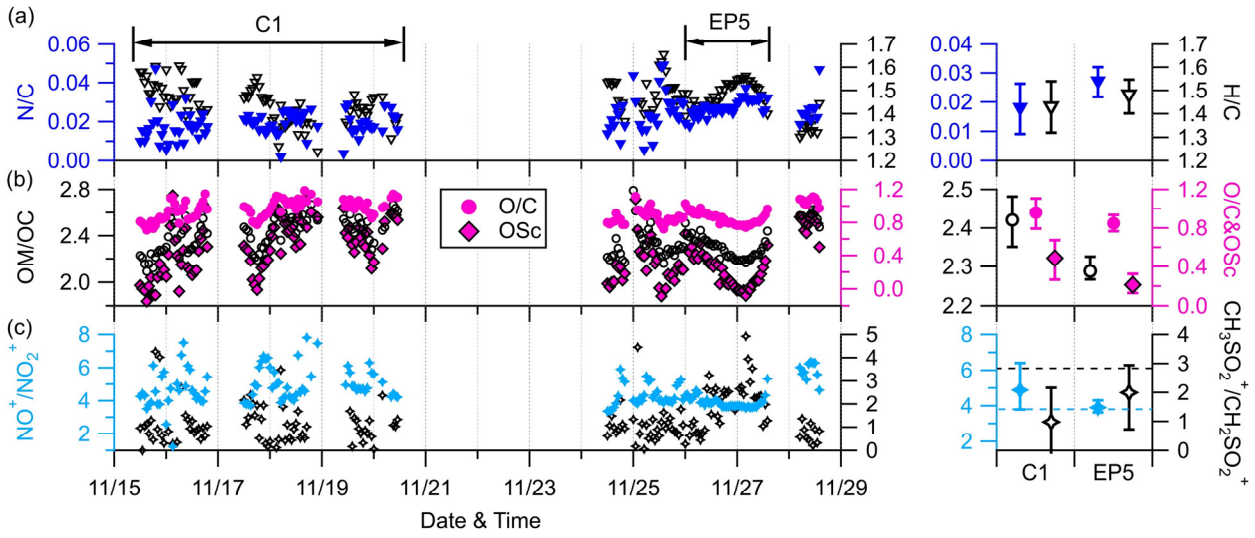

Figure 6. Time series of 1-hour averaged (a) N/C and H/C, (b) OM/OC, OSc, and O/C, and (c) NO^+/NO_2^+ and $CH_3SO_2^+/CH_2SO_2^+$ during the AMS sampling site (left) and their mean values in C1 and EP5 (right). Only ratios determined with good S/N (i.e., organics > 0.7 μg m^{-3}) are shown. The horizontal black and blue dash line in the bottom right plot represent the $CH_3SO_2^+/CH_2SO_2^+$ value for pure MSA (2.9) and the NO^+/NO_2^+ value for pure NH_4NO_3 (3.88), respectively.

3.4 Source apportionment of OA and contribution of organic nitrates

Four factors were resolved by PMF, including three types of SOA and one inorganic factor: less oxidized oxygenated OA (LO-OOA), more oxidized oxygenated OA (MO-OOA), OA associated with sulfate ions (SO_4-OA), and inorganic nitrate

aerosol (NIA). These four factors together on average accounted for 87.5 % of the total NR-PM_1 mass. The mass spectra profiles and OA ion family composition of the four factors are shown in Figs. 7 and 8.

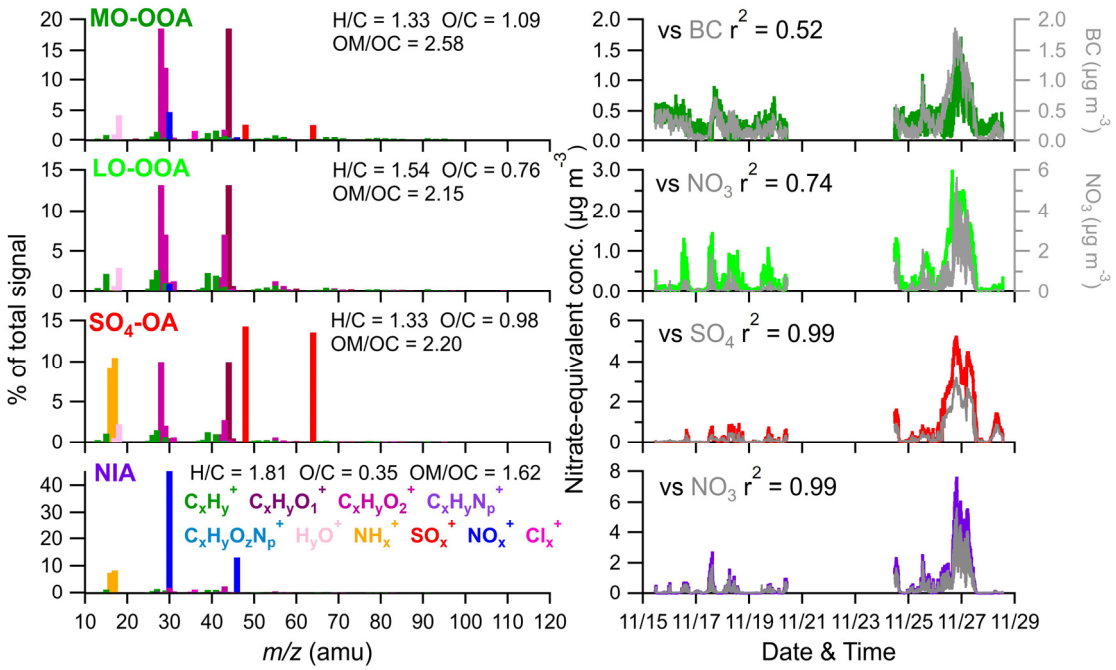

Figure 7. High-resolution mass spectral profiles (left) and time series (right) of four factors. The correlations of four factors with corresponding tracers are also shown.

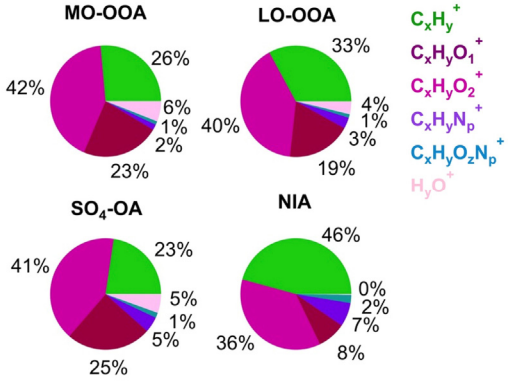

Figure 8. Mass fractional composition of OA ion families for the resolved four PMF factors.

LO-OOA and MO-OOA were identified by prominent peaks of CO^+ and CO_2^+ in the mass spectra. LO-OOA had a high fraction of $C_2H_3O^+$ (*m/z* 43, 6.8 % of the total signal), while MO-OOA, corresponding to more oxidized and aged components, had a higher abundance of CO_2^+ (17.6 % vs. 12.8 %), $C_xH_yO_2^+$ (23 % vs. 19 %), and O/C ratio (1.09 vs. 0.76)

than LO-OOA. The average O/C ratios of these two OOA factors are similar to those at Mt. Bachelor Observatory, where the O/C ratios of SV-OOA and LV-OOA were 0.67 and 1.17, respectively (Zhou et al., 2019). LO-OOA correlate well with NO_3 ($r^2 = 0.74$), coinciding with their secondary nature. Meanwhile, MO-OOA exhibit a moderate correlation with BC ($r^2 = 0.52$), indicating that they were likely coated on BC particles and underwent extensive aging processes during long-range transport. Overall, the LO-OOA and MO-OOA components account for 39.1 % and 29.4 % of the total measured OA mass, respectively (Fig. S11). The mass spectra of the SO_4-OA factor had a large amount of NH_x^+ and SO_x^+, together accounting for 48.5 % of the total mass of this factor. Meanwhile, organic components also made up a considerable fraction, yet on average contributing 51 %. It is also noticed that the O/C ratio of the organic fraction of this factor is 0.98, which is even higher than LO-OOA and comparable to MO-OOA, suggesting that this factor has experienced aging processes during the regional transport. As expected, no primary OA factor (e.g., hydrocarbon-like OA, biomass burning OA, etc.) was resolved during this study due to the negligible influences of local emissions, which was consistent with the PMF results at other background sites (Zhou et al., 2019; Zhu et al., 2016).

An inorganic nitrate aerosol factor was also separated from these OA factors, with nitrates in this factor accounting for 92.6 % of the total NO_x^+ ions. Apart from NIA, NO_x^+ ions were more assigned in MO-OOA (6.0 % of the total NO_x^+) than LO-OOA (1.4 % of the total NO_x^+), suggesting that ONs were more associated with MO-OOA. This is contrary to other studies which reported that ONs were more correlated with less oxidized OA (Zhang et al., 2016; Yu et al., 2019). One possible reason is that ONs formed and mixed with MO-OOA components during the aqueous aging processes of MO-OOA-coated BC particles. This hypothesis is supported by Cao et al. (2022), which demonstrated that ONs exhibit similar volatility to that of MO-OOA when coated on BC. Based on the PMF results above, the mass concentrations of ONs during the AMS sampling period were estimated (Fig. 9). Considering ONs as part of organics, we chose a RIE value of 1.4 for the estimated ONs, while a nitrate RIE value (1.1) was correspondingly applied for INs. The average mass concentration of ONs in C1 was 30 ± 22 ng m^{-3}, which was lower than that in EP5 (40 ± 23 ng m^{-3}), which can also be explained by the evaporative release of ONs in EP5. However, considering the slightly elevated values (10 ng m^{-3}) between these two periods, we cannot rule out the possible formation of ON from aqueous phase processes (Xian et al., 2023) and gas phase reaction initiated by NO_3 during nighttime (Ayres et al., 2015). Also, the low levels of ON might cause uncertainties in its estimation. Since ONs at this site were close to the value (40 ng m^{-3}) reported by Hao et al. (2014) at a forest-urban mixed site in Finland, we considered our quantification of ONs reasonable. However, significant differences were observed between the INs mass concentrations during C1 and EP5 (0.08 μg m^{-3} vs.1.47 μg m^{-3}). This could be attributed to that water-soluble HNO_3 or NH_4NO_3 was scavenged by cloud droplets and removed by precipitation before transporting to this site during C1, while in EP5, these INs dominated the elevation of total nitrate during cloud evaporation. These differences in INs also led to a greater contribution of ONs to total nitrate in C1 than in EP5 (27 % vs. 3 %).

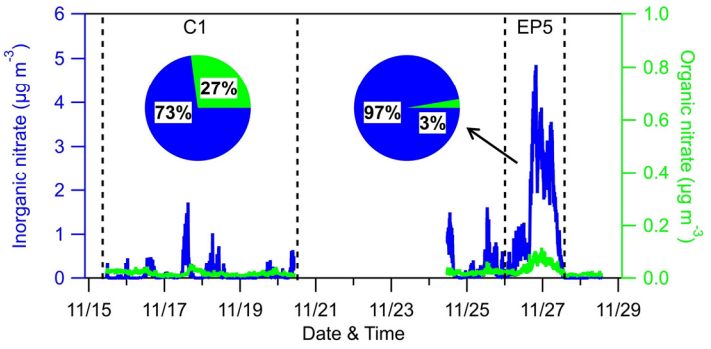

Figure 9. Time series and relative contributions of inorganic nitrate and organic nitrate during the AMS sampling period.

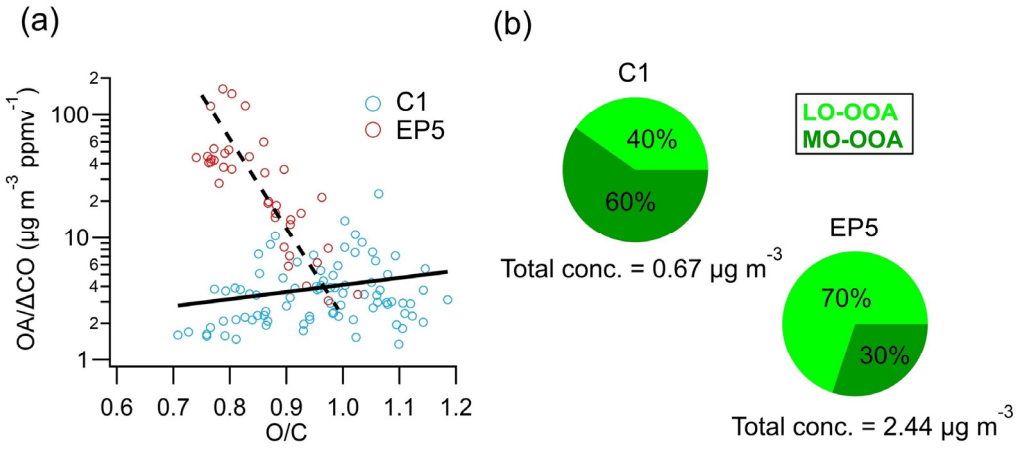

Figure 10. (a) Scatter plot of OA/ΔCO as a function of O/C ratios and (b) mass concentrations and proportions of MO-OOA and LO-OOA during C1 and EP5.

3.5 Evolution of OA

The formation and evolution of OA can be investigated using the ratio of OA to ΔCO (CO minus background CO) to remove the atmospheric dilution effects (Decarlo et al., 2010). In this study, 0.12 ppm (average of the lowest 5 % concentration) was used as the background mixing ratio of CO (Fig. S12), which is close to the 0.1 ppm used in Hu et al. (2013) and Yuan et al. (2013). OA/ΔCO was 28.3 ± 26.3 μg m^{-3} $ppmv^{-1}$ during the study period, which is comparable to (41.7 ± 23.0 μg m^{-3} $ppmv^{-1}$) in suburban Sichuan Basin (Hu et al., 2016) but much lower than the mean value (70 ± 20 μg m^{-3} $ppmv^{-1}$) in worldwide urban air (De Gouw and Jimenez, 2009). The scatter plot of OA/ΔCO as a function of O/C ratios during C1 and EP5 is shown in Fig. 10a. Interestingly, different OA/ΔCO variations were found with the increasing O/C during C1 and EP5. During C1, OA/ΔCO tended to increase with the increase of the O/C ratio, indicating aging process produced SOA (Hu et al., 2017). In contrast, a remarkable decrease trend of OA/ΔCO was observed with the increasing O/C during EP5, suggesting

that less oxidized OA may contribute more significantly to the high OA concentration during this period. Moreover, considering the cloud evaporation process in this period, the negative correlation between OA/ΔCO and O/C in EP5 also implies that the less oxidized OA previously formed or incorporated into cloud droplets can be released during cloud evaporation. Another possible mechanism was that after the cloud was evaporated, SOA formation from biogenic VOCs could then be strengthened by stronger solar radiation, which may also contribute to the increase of less oxidized OA. Conversely, more oxidized OA in cloud droplets may have already undergone mass reduction through fragmentation reactions (Lee et al., 2012), which was far less likely to be reintroduced into the atmosphere. Similarly, significant increases in the LO-OOA concentration (0.27 to 1.70 μg m^{-3}) and fraction (40 % to 70 %) were observed from C1 to EP5, while the MO-OOA concentration (0.40 vs. 0.74 μg m^{-3}) did not show large variation (Fig. 10b), further supporting our conclusion.

Figure 11a shows the Van Krevelen diagrams of OA in this study. The slope of H/C to O/C in the present study was -0.66 (r^2 = 0.64), suggesting the addition of carboxyl functional groups during OA evolution (Heald et al., 2010). This slope is slightly flatter than those (-0.7 to -1.0) of other remote/rural regions across the world (Chen et al., 2015), indicating the oxidation processes of OA at this site were more associated with fragmentation reactions. Consistent evolution trends are also shown in the f_{43} vs. f_{44} space (Fig. 11b). The SO_4-OA and MO-OOA showed similar high oxidation degrees, with f_{43} and f_{44} located at the upper part of the triangular region because of the larger fractional contribution of CO_2^+ in the organic mass spectrum. The LO-OOA was situated in the middle region of the triangle, while NIA resided near the bottom right. Moreover, the mass spectra of LO-OOA and MO-OOA resembles to those of the aged OAs observed at other elevated sites (Xu et al., 2018a; Zhou et al., 2019). These results together reveal that OA observed at SH site is representative of the background-aged SOA in the YRD region in China.

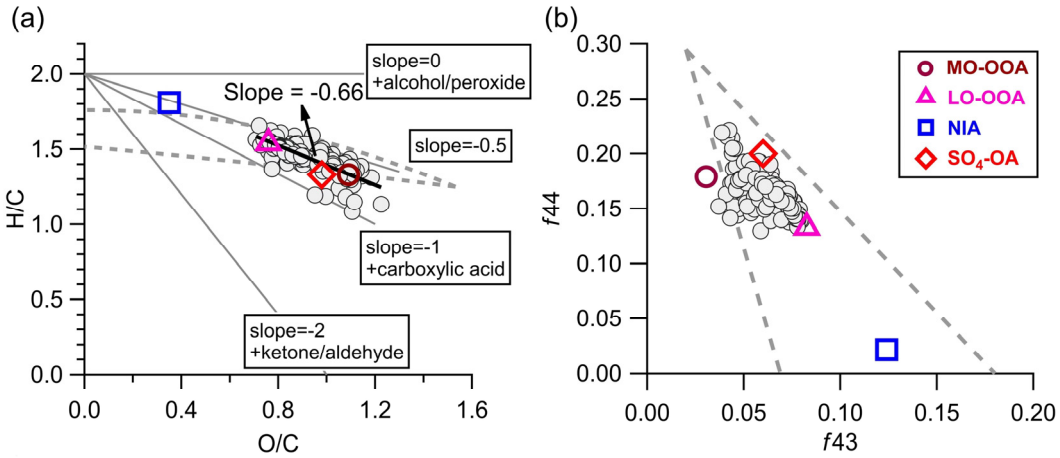

Figure 11. (a) Van Krevelen diagrams (H/C vs. O/C) and (b) f_{43} vs. f_{44} of OA (grey circles, hourly averaged) and four aerosol factors identified by the PMF analyses during the AMS sampling period.

4 Conclusions

Chemical composition and sources of PM_1 at a forested mountain site in southeastern China in November 2022 were characterized by two different aerosol mass spectrometers. The average mass concentration of total PM_1 (4.45 ± 6.51 μg m^{-3}) was overall lower than those at other mountain sites in China, yet it was similarly dominated by organics (41.1 %). Remarkably, sulfate exhibited lower contributions (16.7 %) to PM_1 compared to other mountain sites, in contrast to higher contributions of nitrate (14.7%), indicating the influences of anthropogenic emissions over a relatively small regional scale in southeastern China. Back trajectory analysis revealed that higher concentrations of submicron aerosols at this mountain site were associated with the transport from the western and southwestern regions. OA was dominantly secondary and highly aged as suggested by the high O/C (0.85–0.96) and OSc (0.21–0.49) ratios. PMF analysis of combined organic and inorganic spectra identified two types of OOA and an OA factor associated with SO_4. Most importantly, we found that cloud scavenging and evaporation processes influence LO-OOA and MO-OOA differently. The cloud scavenging showed a greater efficiency in removing MO-OOA, consistent with the smaller size distributions of interstitial particles during cloud events. In contrast, the evaporation of cloud tended to release a large amount of LO-OOA, highlighting that SOA remained in cloud droplets was mostly in a moderate oxidation state. Overall, this study illustrates the importance of SOA in forested mountain site in southeastern China, where aerosol concentrations, composition, size distributions, and oxidation state are affected by aerosol-cloud interactions substantially. Moreover, our study provides valuable data and insights into understanding the aerosol-cloud interactions in mountainous areas that are often under cloudy conditions, and cloud evaporation can be considered as a plausible mechanism to explain certain aerosol episodes in these regions.

Data availability. Data used in this study can be accessed at repository under: https://doi.org/10.5281/zenodo.10312334 (Zhang et al., 2023).

Author contribution. WX and YS designed the research. WX, WZ, and HQ conducted the measurements. ZZ, YZ, WZ, XX, AD, YZ, XC and YS analysed the data. YK, XP, ZW, LL, QF, DRW, and YS reviewed and commented on the paper. ZZ and YS wrote the paper.

Competing interests. DRW is the manufacturer of AMS and ACSM in this study.

utilized in this study. The authors declare that they have no conflict of interest.

Acknowledgements. This work was supported by the National Key Research and Development Program of China (2022YFC3703500), the Strategic Priority Research Program of the Chinese Academy of Sciences (XDB0760200), and the National Natural Science Foundation of China (42377101).

References

Asmi, E., Freney, E., Hervo, M., Picard, D., Rose, C., Colomb, A., and Sellegri, K., Aerosol cloud activation in summer and winter at puy-de-Dôme high altitude site in France. Atmos. Chem. Phys., 12(23), 11589-607, https://doi.org/10.5194/acp-12-11589-2012, 2012.

Ayres, B. R., Allen, H. M., Draper, D. C., Brown, S. S., Wild, R. J., Jimenez, J. L., Day, D. A., Campuzano-Jost, P., Hu, W., de Gouw, J., Koss, A., Cohen, R. C., Duffey, K. C., Romer, P., Baumann, K., Edferton, E., Takahama, S., Thornton, J. A., Lee, B. H., Lopez-Hilfiker, F. D., Mohr, C., Wennberg, P. O., Nguyen, T. B., Teng, A., Goldstein, A. H., Olson, K., and Fry, J. L.: Organic nitrate aerosol formation via NO_3 + biogenic volatile organic compounds in the southeastern United States. Atmos. Chem. Phys., 15(23), 13377-92, https://doi.org/10.5194/acp-15-13377-2015, 2015.

Brown, S. S., Ryerson, T. B., Wollny, A. G., Brock, C. A., Peltier, R., Sullivan, A. P., Weber, R. J., Dubé, W. P., Trainer, M., Meagher, J. F., Fehsenfeld, F. C., and Ravishankara, A. R.: Variability in Nocturnal Nitrogen Oxide Processing and Its Role in Regional Air Quality. Science, 311(5757), 67-70, https://doi.org/10.1126/science.1120120, 2006.

Calvo, A. I., Alves, C., Castro, A., Pont, V., Vicente, A. M., and Fraile, R.: Research on aerosol sources and chemical composition: Past, current and emerging issues, Atmos. Res., 120-121, 1-28, https://doi.org/10.1016/j.atmosres.2012.09.021, 2013.

Canagaratna, M. R., Jayne, J. T., Jimenez, J. L., Allan, J. D., Alfarra, M. R., Zhang, Q., Onasch, T. B., Drewnick, F., Coe, H., Middlebrook, A., Delia, A., Williams, L. R., Trimborn, A. M., Northway, M. J., DeCarlo, P. F., Kolb, C. E., Davidovits, P., and Worsnop, D. R.: Chemical and microphysical characterization of ambient aerosols with the aerodyne aerosol mass spectrometer. Mass Spectrom. Rev., 26(2), 185-222, https://doi.org/10.1002/mas.20115, 2007.

Canagaratna, M. R., Jimenez, J. L., Kroll, J. H., Chen, Q., Kessler, S. H., Massoli, P., Hildebrandt Ruiz, L., Fortner, E., Williams, L. R., Wilson, K. R., Surratt, J. D., Donahue, N. M., Jayne, J. T., and Worsnop, D. R.: Elemental ratio measurements of organic compounds using aerosol mass spectrometry: characterization, improved calibration, and implications, Atmos. Chem. Phys., 15, 253-272, https://doi.org/10.5194/acp-15-253-2015, 2015.

Cao, L.-M., Wei, J., He, L.-Y., Zeng, H., Li, M.-L., Zhu, Q., Yu, G. H., and Huang, X. F.: Aqueous aging of secondary organic aerosol coating onto black carbon: Insights from simultaneous L-ToF-AMS and SP-AMS measurements at an urban site in southern China. J. Clean. Prod., 330, 129888, https://doi.org/10.1016/j.jclepro.2021.129888, 2022.

Carbone, C., Decesari, S., Paglione, M., Giulianelli, L., Rinaldi, M., Marinoni, A., Cristofanelli, P., Didiodato, A., Bonasoni, P., Fuzzi, S., and Facchini, M. C.: 3-year chemical composition of free tropospheric PM1 at the Mt. Cimone GAW global station – South Europe – 2165 m a.s.l, Atmos. Environ., 87, 218-227, https://doi.org/10.1016/j.atmosenv.2014.01.048, 2014.

Chen, Q., Heald, C. L., Jimenez, J. L., Canagaratna, M. R., Zhang, Q., He, L.-Y., Huang, X.-F., Campuzano-Jost, P., Palm, B. B., Poulain, L., Kuwara, M., Martin, S. T., Abbatt, J. P. D., Lee, A. K. Y., and Liggio, J.: Elemental composition of

organic aerosol: The gap between ambient and laboratory measurements. Geophys. Res. Lett., 42(10), 4182-9, https://doi.org/10.1002/2015GL063693, 2015.

Chen, Y., Xu, L., Humphry, T., Hettiyadura, A. P. S., Ovadnevaite, J., Huang, S., Poulain, L., Schroder, J. C., Campuzano-Jost, P., Jimenez, J. L., Herrmann, H., O'Dowd, C., Stone, E. A., and Ng, N. L.: Response of the Aerodyne Aerosol Mass Spectrometer to Inorganic Sulfates and Organosulfur Compounds: Applications in Field and Laboratory Measurements, Environ. Sci. Technol., 53, 5176-5186, https://doi.org/10.1021/acs.est.9b00884, 2019.

De Gouw, J. and Jimenez, J. L.: Organic Aerosols in the Earth's Atmosphere, Environ. Sci. Technol., 43, 7614-7618, https://doi.org/10.1021/es9006004, 2009.

DeCarlo, P. F., Ulbrich, I. M., Crounse, J., de Foy, B., Dunlea, E. J., Aiken, A. C., Knapp, D., Weinheimer, A. J., Campos, T., Wennberg, P. O., and Jimenez, J. L.: Investigation of the sources and processing of organic aerosol over the Central Mexican Plateau from aircraft measurements during MILAGRO. Atmos. Chem. Phys., 10(12), 5257-80, https://doi.org/10.5194/acp-10-5257-2010, 2010.

Ding, S., Liu, D., Hu, K., Zhao, D., Tian, P., Wang, F., Li, R., Chen, Y., He, H., Huang, M., and Ding, D.: Optical and hygroscopic properties of black carbon influenced by particle microphysics at the top of the anthropogenically polluted boundary layer, Atmos. Chem. Phys., 21, 681-694, https://doi.org/10.5194/acp-21-681-2021, 2021.

Du, W., Sun, Y. L., Xu, Y. S., Jiang, Q., Wang, Q. Q., Yang, W., Wang, F., Bai, Z. P., Zhao, X. D., and Yang, Y. C.: Chemical characterization of submicron aerosol and particle growth events at a national background site (3295 m a.s.l.) on the Tibetan Plateau, Atmos. Chem. Phys., 15, 10811-10824, https://doi.org/10.5194/acp-15-10811-2015, 2015.

Farmer, D. K., Matsunaga, A., Docherty, K. S., Surratt, J. D., Seinfeld, J. H., Ziemann, P. J., and Jimenez, J. L.: Response of an aerosol mass spectrometer to organonitrates and organosulfates and implications for atmospheric chemistry, P. Natl. Acad. Sci. USA, 107, 6670-6675, https://doi.org/10.1073/pnas.0912340107, 2010.

Fry, J. L., Kiendler-Scharr, A., Rollins, A. W., Wooldridge, P. J., Brown, S. S., Fuchs, H., Dubé, W., Mensah, A., dal Maso, M., Tillmann, R., Dorn, H. P., Brauers, T., and Cohen, R. C.: Organic nitrate and secondary organic aerosol yield from NO_3 oxidation of β-pinene evaluated using a gas-phase kinetics/aerosol partitioning model, Atmos. Chem. Phys., 9, 1431-1449, https://doi.org/10.5194/acp-9-1431-2009, 2009.

Fry, J. L., Draper, D. C., Zarzana, K. J., Campuzano-Jost, P., Day, D. A., Jimenez, J. L., Brown, S. S., Cohen, R. C., Kaser, L., Hansel, A., Cappellin, L., Karl, T., Hodzic Roux, A., Turnipseed, A., Cantrell, C., Lefer, B. L., and Grossberg, N.: Observations of gas- and aerosol-phase organic nitrates at BEACHON-RoMBAS 2011, Atmos. Chem. Phys., 13, 8585-8605, https://doi.org/10.5194/acp-13-8585-2013, 2013.

Gao, M., Zhou, S. Z., He, Y., Zhang, G. H., Ma, N., Li, Y., Li, F. H., Yang, Y. X., Peng, L., Zhao, J., Bi, X. H., Hu, W. W., Sun, Y. L., Wang, B. G., and Wang, X. M.: In Situ Observation of Multiphase Oxidation-Driven Secondary Organic Aerosol Formation during Cloud Processing at a Mountain Site in Southern China, Environ. Sci. Technol. Lett., 10, 573-581, https://doi.org/10.1021/acs.estlett.3c00331, 2023.

Ge, X. L., Zhang, Q., Sun, Y. L., Ruehl, C. R., and Setyan, A.: Effect of aqueous-phase. processing on aerosol chemistry and size distributions in Fresno, California, during wintertime, Environ. Chem., 9, 221-235, 2012.

Gelaro, R., McCarty, W., Suárez, M. J., Todling, R., Molod, A., Takacs, L., Randles, C. A., Darmenov, A., Bosilovich, M. G., Reichle, R., Wargan, K., Coy, L., Cullather, R., Draper, C., Akella, S., Buchard, V., Conaty, A., de Silva, A. M., Gu, W., Kim, G.-K., Koster, R., Merkova, D., Nielsen, J. E., Partyka, G., Pawson, S., Putman, W., Rienecker, W., Rienecker, M., Schubert, S. D., Sienkiewicz, M., and Zhao, B.: The Modern-Era Retrospective Analysis for Research and Applications, Version 2 (MERRA-2). J. Climate, 30(14), 5419-54, https://doi.org/10.1175/JCLI-D-16-0758.1, 2017.

Gilardoni, S., Massoli, P., Giulianelli, L., Rinaldi, M., Paglione, M., Pollini, F., Lanconelli, C., Poluzzi, V., Carbone, S., Hillamo, R., Russell, L. M., Facchini, M. C., and Fuzzi, S.: Fog scavenging of organic and inorganic aerosol in the Po Valley, Atmos. Chem. Phys., 14, 6967-6981, https://doi.org/10.5194/acp-14-6967-2014, 2014.

Hallquist, M., Wenger, J. C., Baltensperger, U., Rudich, Y., Simpson, D., Claeys, M., Dommen, J., Donahue, N. M., George, C., Goldstein, A. H., Hamilton, J. F., Herrmann, H., Hoffmann, T., Iinuma, Y., Jang, M., Jenkin, M. E., Jimenez, J. L., Kiendler-Scharr, A., Maenhaut, W., McFiggans, G., Mentel, T. F., Monod, A., Prevot, A. S. H., Seinfeld, J. H., Surratt, J. D., Szmigielski, R., and Wildt, J.: The formation, properties and impact of secondary organic aerosol: current and emerging issues, Atmos. Chem. Phys., 9, 5155-5236, https://doi.org/10.5194/acp-9-5155-2009, 2009.

Hao, L. Q., Kortelainen, A., Romakkaniemi, S., Portin, H., Jaatinen, A., Leskinen, A., Komppula, M., Miettinen, P., Sueper, D., Pajunoja, A., Smith, J. N., Lehtinen, K. E. J., Worsnop, D. R., Laaksonen, A., and Virtanen, A.: Atmospheric submicron aerosol composition and particulate organic nitrate formation in a boreal forestland–urban mixed region, Atmos. Chem. Phys., 14, 13483-13495, https://doi.org/10.5194/acp-14-13483-2014, 2014.

Haywood, J. and Boucher, O.: Estimates of the direct and indirect radiative forcing. due to tropospheric aerosols: A review, Rev. Geophys., 38, 513-543, https://doi.org/10.1029/1999rg000078, 2000.

Heald, C. L., Kroll, J. H., Jimenez, J. L., Docherty, K. S., DeCarlo, P. F., Aiken, A. C., Chen, Q., Martin, S. T., Farmer, D. K., and Artaxo, P.: A simplified description of the evolution of organic aerosol composition in the atmosphere, Geophys. Res. Lett., 37, https://doi.org/10.1029/2010GL042737, 2010.

Hu, W., Hu, M., Hu, W. W., Zheng, J., Chen, C., Wu, Y., and Guo, S.: Seasonal variations in high time-resolved chemical compositions, sources, and evolution of atmospheric submicron aerosols in the megacity Beijing, Atmos. Chem. Phys., 17, 9979-10000, https://doi.org/10.5194/acp-17-9979-2017, 2017.

Hu, W., Hu, M., Hu, W. W., Niu, H., Zheng, J., Wu, Y., Chen, W., Chen, C., Li, L., Shao, M., Xie, S., and Zhang, Y.: Characterization of submicron aerosols influenced by biomass burning at a site in the Sichuan Basin, southwestern China, Atmos. Chem. Phys., 16, 13213-13230, https://doi.org/10.5194/acp-16-13213-2016, 2016.

Hu, W. W., Hu, M., Yuan, B., Jimenez, J. L., Tang, Q., Peng, J. F., Hu, W., Shao, M., Wang, M., Zeng, L. M., Wu, Y. S., Gong, Z. H., Huang, X. F., and He, L. Y.: Insights on organic aerosol aging and the influence of coal combustion at a regional receptor site of central eastern China, Atmos. Chem. Phys., 13, 10095-10112, 10.5194/acp-13-10095-2013, 2013.

Huang, R. J., Zhang, Y. L., Bozzetti, C., Ho, K. F., Cao, J. J., Han, Y. M., Daellenbach, K. R., Slowik, J. G., Platt, S. M., Canonaco, F., Zotter, P., Wolf, R., Pieber, S. M., Bruns, E. A., Crippa, M., Ciarelli, G., Piazzalunga, A., Schwikowski, M., Abbaszade, G., Schnelle-Kreis, J., Zimmermann, R., An, Z. S., Szidat, S., Baltensperger, U., El Haddad, I., and Prevot, A. S. H.: High secondary aerosol contribution to particulate pollution during haze events in China, Nature, 514, 218-222, https://doi.org/10.1038/nature13774, 2014.

Huang, W., Yang, Y., Wang, Y. H., Gao, W. K., Li, H. Y., Zhang, Y. Y., Li, J. Y, Zhao, S. M, Yan, Y. C, Ji, D. S, Tang, G. Q., Liu, Z. R., Wang, L. L., Zhang, R. J, and Wang, Y. S.: Exploring the inorganic and organic nitrate aerosol formation regimes at a suburban site on the North China Plain, Sci. Total Environ., 768, 144538, https://doi.org/10.1016/j.scitotenv.2020.144538, 2021.

Huang, X., Ding, A. J., Wang, Z. L., Ding, K., Gao, J., Chai, F. H., and Fu, C. B.: Amplified transboundary transport of haze by aerosol-boundary layer interaction in China, Nat. Geosci., 13, 428-434, https://doi.org/10.1038/s41561-020-0583-4, 2020.

Kampa, M. and Castanas, E.: Human health effects of air pollution, Environ. Pollut., 151, 362-367, https://doi.org/10.1016/j.envpol.2007.06.012, 2008.

Kanakidou, M., Seinfeld, J. H., Pandis, S. N., Barnes, I., Dentener, F. J., Facchini, M. C., Van Dingenen, R., Ervens, B., Nenes, A., Nielsen, C. J., Swietlicki, E., Putaud, J. P., Balkanski, Y., Fuzzi, S., Horth, J., Moortgat, G. K., Winterhalter, R., Myhre, C. E. L., Tsigaridis, K., Vignati, E., Stephanou, E. G., and Wilson, J.: Organic aerosol and global climate modelling: a review, Atmos. Chem. Phys., 5, 1053-1123, https://doi.org/10.5194/acp-5-1053-2005, 2005.

Kuang, Y., Xu, W., Tao, J., Luo, B., Liu, L., Xu, H., Xu, W., Xue, B., Zhai, M., Liu, P., and Sun, Y.: Divergent Impacts of Biomass Burning and Fossil Fuel Combustion Aerosols on Fog-Cloud Microphysics and Chemistry: Novel Insights From Advanced Aerosol-Fog Sampling, Geophys. Res. Lett., 51, e2023GL107147, https://doi.org/10.1029/2023GL107147, 2024.

Lee, A. K. Y., Hayden, K. L., Herckes, P., Leaitch, W. R., Liggio, J., Macdonald, A. M., and Abbatt, J. P. D.: Characterization of aerosol and cloud water at a mountain site during WACS 2010: secondary organic aerosol formation through oxidative cloud processing. Atmos. Chem. Phys., 12(15), 7103-16, https://doi.org/10.5194/acp-12-7103-2012, 2012.

Li, J. J., Wang, G. H., Cao, J. J., Wang, X. M., and Zhang, R. J.: Observation of. biogenic secondary organic aerosols in the atmosphere of a mountain site in central China: temperature and relative humidity effects, Atmos. Chem. Phys., 13, 11535-11549, https://doi.org/10.5194/acp-13-11535-2013, 2013.

Li, Z. Y., Xie, P. H, Hu, R. Z., Wang, D., Jin, H. W., Chen, H., Lin, C., and Liu, W. Q: Observations of N_2O_5 and NO_3 at a suburban environment in Yangtze river delta in China: Estimating heterogeneous N_2O_5 uptake coefficients. J. Environ. Sci., 95, 248-55, https://doi.org/10.1016/j.jes.2020.04.041, 2020.

Lin, C., Huang, R.-J., Duan, J., Zhong, H., and Xu, W.: Primary and Secondary Organic Nitrate in Northwest China: A Case Study, Environ. Sci. Technol. Lett., 8, 947-953, https://doi.org/10.1021/acs.estlett.1c00692, 2021.

Middlebrook, A. M., Bahreini, R., Jimenez, J. L., and Canagaratna, M. R.: Evaluation of Composition-Dependent Collection Efficiencies for the Aerodyne Aerosol Mass Spectrometer using Field Data, Aerosol Sci. and Techno., 46, 258-271, https://doi.org/10.1080/02786826.2011.620041, 2012.

Monks, P. S., Granier, C., Fuzzi, S., Stohl, A., Williams, M. L., Akimoto, H., Amann, M., Baklanov, A., Baltensperger, U., Bey, I., Blake, N., Blake, R. S., Carslaw, K., Cooper, O. R., Dentener, F., Fowler, D., Fragkou, E., Frost, G. J., Generoso, S., Ginoux, P., Grewe, V., Guenther, A., Hansson, H. C., Henne, S., Hjorth, J., Hofzumahaus, A., Huntrieser, H., Isaksen, I. S. A., Jenkin, M. E., Kaiser, J., Kanakidou, M., Klimont, Z., Kulmala, M., Laj, P., Lawrence, M. G., Lee, J. D., Liousse, C., Maione, M., McFiggans, G., Metzger, A., Mieville, A., Moussiopoulos, N., Orlando, J. J., O'Dowd, C. D., Palmer, P. I., Parrish, D. D., Petzold, A., Platt, U., Pöschl, U., Prévôt, A. S. H., Reeves, C. E., Reimann, S., Rudich, Y., Sellegri, K., Steinbrecher, R., Simpson, D., ten Brink, H., Theloke, J., van der Werf, G. R., Vautard, R., Vestreng, V., Vlachokostas, C., and von Glasow, R.: Atmospheric composition change – global and regional air quality, Atmos. Environ., 43, 5268-5350, https://doi.org/10.1016/j.atmosenv.2009.08.021, 2009.

Nault, B. A., Croteau, P., Jayne, J., Williams, A., Williams, L., Worsnop, D. R., Katz, E. F., DeCarlo, P. F., and Canagaratna, M.: Laboratory evaluation of organic aerosol relative ionization efficiencies in the aerodyne aerosol mass spectrometer and aerosol chemical speciation monitor. Aerosol Sci. Techno., 57(10), 981-97, https://doi.org/10.1080/02786826.2023.2223249, 2023.

Pokorná, P., Zíková, N., Vodička, P., Lhotka, R., Mbengue, S., Holubová Šmejkalová, A., Riffault, V., Ondráček, J., Schwarz, J., and Ždímal, V.: Chemically speciated mass size distribution, particle density, shape and origin of non-refractory PM_1 measured at a rural background site in central Europe, Atmos. Chem. Phys., 22, 5829-5858, https://doi.org/10.5194/acp-22-5829-2022, 2022.

Ramanathan, V., Crutzen, P. J., Kiehl, J. T., and Rosenfeld, D.: Atmosphere - Aerosols, climate, and the hydrological cycle, Science, 294, 2119-2124, https://doi.org/10.1126/science.1064034, 2001.

Rejano, F., Titos, G., Casquero-Vera, J. A., Lyamani, H., Andrews, E., Sheridan, P., Cazorla, A., Castillo, S., Alados-Arboledas, L., and Olmo, F.: Activation properties of aerosol particles as cloud condensation nuclei at urban and high-altitude remote sites in southern Europe. Sci. Tot. Environ., 762, 143100, https://doi.org/10.1016/j.scitotenv.2020.143100, 2021.

Roth, A., Schneider, J., Klimach, T., Mertes, S., van Pinxteren, D., Herrmann, H., and Borrmann, S.: Aerosol properties, source identification, and cloud processing in orographic clouds measured by single particle mass spectrometry on a central European mountain site during HCCT-2010. Atmos Chem Phys., 16(2), 505-24, https://doi.org/10.5194/acp-16-505-2016, 2016.

Song, S. J., Gao, M., Xu, W. Q., Sun, Y. L., Worsnop, D. R., Jayne, J. T., Zhang, Y. Z., Zhu, L., Li, M., Zhou, Z., Cheng, C. L., Lv, Y. B., Wang, Y., Peng, W., Xu, X. B., Lin, N., Wang, Y. X., Wang, S. X., Munger, J. W., Jacob, D. J., and McElroy, M. B.: Possible heterogeneous chemistry of hydroxymethanesulfonate (HMS) in northern China winter haze, Atmos. Chem. Phys., 19, 1357-1371, https://doi.org/10.5194/acp-19-1357-2019, 2019.

Sun, Y. L., Zhang, Q., Schwab, J. J., Yang, T., Ng, N. L., and Demerjian, K. L.: Factor analysis of combined organic and inorganic aerosol mass spectra from high resolution aerosol mass spectrometer measurements, Atmos. Chem. Phys., 12, 8537-8551, https://doi.org/10.5194/acp-12-8537-2012, 2012.

Sun, Y. L., Zhang, Q., Schwab, J. J., Chen, W. N., Bae, M. S., Lin, Y. C., Hung, H. M., and Demerjian, K. L.: A case study of aerosol processing and evolution in summer in New York City, Atmos. Chem. Phys., 11, 12737-12750, https://doi.org/10.5194/acp-11-12737-2011, 2011.

Tang, C. G., Zhang, X. H., Tian, P. F., Guan, X., Lin, Y. J., Pang, S. T., Guo, Q., Du, T., Zhang, Z. D, Zhang, M., Xu, J. Z., and Zhang, L.: Chemical characteristics and regional transport of submicron particulate matter at a suburban site near Lanzhou, China, Environ. Res., 212, 113179, https://doi.org/10.1016/j.envres.2022.113179, 2022.

Tang, L. L, Yu, H. X., Ding, A. J, Zhang, Y. J., Qin, W., Wang, Z., Chen, W. T, Hua, Y., and Yang, X. X.: Regional contribution to PM_1 pollution during winter haze in Yangtze River Delta, China, Sci. Total Environ., 541, 161-166, https://doi.org/10.1016/j.scitotenv.2015.05.058, 2016.

Tao, J., Zhang, Z. S., Tan, H. B., Zhang, L. M., Wu, Y. F., Sun, J. R., Che, H. Z., Cao, J. J., Cheng, P., Chen, L. G., and Zhang, R. J.: Observational evidence of cloud processes contributing to daytime elevated nitrate in an urban atmosphere, Atmos. Environ., 186, 209-215, https://doi.org/10.1016/j.atmosenv.2018.05.040, 2018.

Ulbrich, I. M., Canagaratna, M. R., Zhang, Q., Worsnop, D. R., and Jimenez, J. L.: Interpretation of organic components from Positive Matrix Factorization of aerosol mass spectrometric data, Atmos. Chem. Phys., 9, 2891-2918, https://doi.org/10.5194/acp-9-2891-2009, 2009.

Wang, J. F., Ge, X. L, Chen, Y. F., Shen, Y. F., Zhang, Q., Sun, Y. L., Xu, J. Z., Ge, S., Yu, H., and Chen, M. D.: Highly time-resolved urban aerosol characteristics during springtime in Yangtze River Delta, China: insights from soot particle aerosol mass spectrometry, Atmos. Chem. Phys., 16, 9109-9127, https://doi.org/10.5194/acp-16-9109-2016, 2016.

Wang, Q. Y., Huang, R. J., Cao, J. J., Tie, X. X., Ni, H. Y., Zhou, Y. Q., Han, Y. M., Hu, T. F., Zhu, C. S., Feng, T., Li, N., and Li, J. D.: Black carbon aerosol in winter northeastern Qinghai–Tibetan Plateau, China: the source, mixing state and optical property, Atmos. Chem. Phys., 15, 13059-13069, https://doi.org/10.5194/acp-15-13059-2015, 2015.

Wen, L., Xue, L. K., Dong, C., Wang, X. F., Chen, T. S., Jiang, Y., Gu, R. R., Zheng, P. G., Li, H. Y., Shan, Y., Zhu, Y. J., Zhao, Y., Yin, X. K., Liu, H. D., Gao, J., Wu, Z. J., Wang, T., Herrmann, H., and Wang, W. X.: Reduced atmospheric sulfate enhances fine particulate nitrate formation in eastern China. Sci. Total Environ., 898, 165303, https://doi.org/10.1016/j.scitotenv.2023.165303, 2023.

Xian, J., Cui, S., Chen, X., Wang, J., Xiong, Y., Gu, C., Wang, Y., Zhang, Y. J., Li, H. W., Wang, J. F., and Ge, X. L.: Online chemical characterization of atmospheric fine secondary aerosols and organic nitrates in summer Nanjing, China. Atmos. Res., 290, 106783, https://doi.org/10.1016/j.atmosres.2023.106783, 2023.

Xu, J., Zhang, Q., Chen, M., Ge, X., Ren, J., and Qin, D.: Chemical composition, sources, and processes of urban aerosols during summertime in northwest China: insights from high-resolution aerosol mass spectrometry, Atmos. Chem. Phys., 14, 12593-12611, https://doi.org/10.5194/acp-14-12593-2014, 2014.

Xu, J. Z., Zhang, Q., Shi, J. S., Ge, X. L., Xie, C. H., Wang, J. F., Kang, S. C., Zhang, R. X., and Wang, Y. H.: Chemical characteristics of submicron particles at the central Tibetan Plateau: insights from aerosol mass spectrometry, Atmos. Chem. Phys., 18, 427-443, https://doi.org/10.5194/acp-18-427-2018, 2018a.

Xu, L., Suresh, S., Guo, H., Weber, R. J., and Ng, N. L.: Aerosol characterization over. the southeastern United States using high-resolution aerosol mass spectrometry: spatial and seasonal variation of aerosol composition and sources with a focus on organic nitrates, Atmos. Chem. Phys., 15, 7307-7336, https://doi.org/10.5194/acp-15-7307-2015, 2015.

Xu, P., Zhang, J. K., Ji, D. S., Liu, Z. R., Tang, G. Q., Jiang, C. S., and Wang, Y. S.: Characterization of submicron particles during autumn in Beijing, China, J. Environ. Sci., 63, 16-27, https://doi.org/10.1016/j.jes.2017.03.036, 2018b.

Yu, K., Zhu, Q., Du, K., and Huang, X. F.: Characterization of nighttime formation of particulate organic nitrates based on high-resolution aerosol mass spectrometry in an urban atmosphere in China. Atmos. Chem. Phys., 19(7), 5235-49, https://doi.org/10.5194/acp-19-5235-2019, 2019.

Yuan, B., Hu, W. W., Shao, M., Wang, M., Chen, W. T., Lu, S. H., Zeng, L. M., and. Hu, M.: VOC emissions, evolutions and contributions to SOA formation at a receptor site in eastern China, Atmos. Chem. Phys., 13, 8815-8832, https://doi.org/10.5194/acp-13-8815-2013, 2013.

Zhang, Q., Jimenez, J. L., Canagaratna, M. R., Ulbrich, I. M., Ng, N. L., Worsnop, D. R., and Sun, Y. L.: Understanding atmospheric organic aerosols via factor analysis of aerosol mass spectrometry: a review, Anal. Bioanal. Chem., 401, 3045-3067, https://doi.org/10.1007/s00216-011-5355-y, 2011.

Zhang, X. H., Xu, J. Z., Kang, S. C., Liu, Y. M., and Zhang, Q.: Chemical characterization of long-range transport biomass burning emissions to the Himalayas: insights from high-resolution aerosol mass spectrometry, Atmos. Chem. Phys., 18, 4617-4638, https://doi.org/10.5194/acp-18-4617-2018, 2018.

Zhang, X. H., Xu, J. Z., Kang, S. C., Zhang, Q., and Sun, J. Y.: Chemical characterization and sources of submicron aerosols in the northeastern Qinghai–Tibet Plateau: insights from high-resolution mass spectrometry, Atmos. Chem. Phys., 19, 7897-7911, https://doi.org/10.5194/acp-19-7897-2019, 2019.

Zhang, Y. J., Tang, L. L., Wang, Z., Yu, H. X., Sun, Y. L., Liu, D., Qin, W., Canonaco, F., Prévôt, A. S. H., Zhang, H. L., and Zhou, H. C.: Insights into characteristics, sources, and evolution of submicron aerosols during harvest seasons in the Yangtze River delta region, China, Atmos. Chem. Phys., 15, 1331-1349, https://doi.org/10.5194/acp-15-1331-2015, 2015.

Zhang, J. K., Cheng, M. T., Ji, D. S., Liu, Z. R., Hu, B., Sun, Y. L., Wang, Y. S.: Characterization of submicron particles during biomass burning and coal combustion periods in Beijing, China. Sci. Total Environ., 562, 812-21, https://doi.org/10.1016/j.scitotenv.2016.04.015, 2016.

Zhang, Y. M., Zhang, X. Y., Sun, J. Y., Hu, G. Y., Shen, X. J., Wang, Y. Q., Wang, T. T., Wang, D. Z., and Zhao, Y.: Chemical composition and mass size distribution of PM_1 at an elevated site in central east China, Atmos. Chem. Phys., 14, 12237-12249, https://doi.org/10.5194/acp-14-12237-2014, 2014.

Zheng, J., Hu, M., Du, Z. F., Shang, D. J., Gong, Z. H., Qin, Y. H., Fang, J. Y., Gu, F. T., Li, M. R., Peng, J. F., Li, J., Zhang, Y. Q., Huang, X. F., He, L. Y., Wu, Y. S., and Guo, S.: Influence of biomass burning from South Asia at a high-altitude mountain receptor site in China, Atmos. Chem. Phys., 17, 6853-6864, https://doi.org/10.5194/acp-17-6853-2017, 2017.

Zhong, H. B., Huang, R.-J., Lin, C. S., Xu, W., Duan, J., Gu, Y. F., Huang, W., Ni, H. Y., Zhu, C. S., You, Y., Wu, Y. F., Zhang, R. J., Ovadnevaite, J., Ceburnis, D., and O'Dowd, C. D.: Measurement report: On the contribution of long-distance transport to the secondary aerosol formation and aging, Atmos. Chem. Phys., 22, 9513-9524, https://doi.org/10.5194/acp-22-9513-2022, 2022.

Zhou, S., Collier, S., Jaffe, D. A., and Zhang, Q.: Free tropospheric aerosols at the Mt. Bachelor Observatory: more oxidized and higher sulfate content compared to boundary layer aerosols, Atmos. Chem. Phys., 19, 1571-1585, https://doi.org/10.5194/acp-19-1571-2019, 2019.

Zhou, W., Xu, W. Q, Kim, H., Zhang, Q., Fu, P. Q., Worsnop, D. R., and Sun, Y. L.: A review. of aerosol chemistry in Asia: insights from aerosol mass spectrometer measurements, Environ. Sci.-Proc. Imp., 22, https://doi.org/1616-1653, 10.1039/D0EM00212G, 2020.

Zhu, Q., He, L. Y., Huang, X. F., Cao, L. M., Gong, Z. H., Wang, C., Zhuang, X., and Hu, M.: Atmospheric aerosol compositions and sources at two national background sites in northern and southern China, Atmos. Chem. Phys., 16, 10283-10297, https://doi.org/10.5194/acp-16-10283-2016, 2016.